3D geometrical characterization and modelling of solid oxide cells electrodes microstructure by image analysis

Hamza Moussaoui, Johan Debayle, Yann Gavet, Gérard Delette, Maxime Hubert, Peter Cloetens, Jérôme Laurencin

3D geometrical characterization and modelling of solid oxide cells electrodes microstructure by image analysis

H. Moussaoui[*a,b,c], J. Debayle[c], Y. Gavet[c], G. Delette[b], M. Hubert[a,b,d], P. Cloetens[d], J. Laurencin[b]
[a]Univ. Grenoble Alpes, F-38000 Grenoble, France
[b]CEA, LITEN - CEA Grenoble, 38054 Grenoble Cedex 9, France
[c]Ecole des Mines de Saint-Etienne, SPIN, CNRS 5307, LGF, F-42023 Saint-Etienne, France
[d]European Synchrotron Radiation Facility (ESRF), 71 avenue des Martyrs, 38000, Grenoble, France

ABSTRACT

A strong correlation exists between the performance of Solid Oxide Cells (SOCs), working either in fuel cell or electrolysis mode, and their electrodes microstructure. However, the basic relationships between the three-dimensional characteristics of the microstructure and the electrode properties are not still precisely understood. Thus, several studies have been recently proposed in an attempt to improve the knowledge of such relations, which are essential before optimizing the microstructure, and hence, designing more efficient SOC electrodes. In that frame, an original model has been adapted to generate virtual 3D microstructures of typical SOCs electrodes. Both the oxygen electrode, which is made of porous LSCF, and the hydrogen electrodes, made of porous Ni-YSZ, have been studied. In this work, the synthetic microstructures are generated by the so-called 3D Gaussian 'Random Field model'. The morphological representativeness of the virtual porous media have been validated on real 3D electrode microstructures of a commercial cell, obtained by X-ray nano-tomography at the European Synchrotron Radiation Facility (ESRF). This validation step includes the comparison of the morphological parameters like the phase covariance function and granulometry as well as the physical parameters like the 'apparent tortuosity'. Finally, this validated tool will be used, in forthcoming studies, to identify the optimal microstructure of SOCs.

Keywords: SOC, Fuel cells, Microstructure modelling, 3D Gaussian random field model, LSCF, Ni-YSZ, X-ray nano-tomography.

1. INTRODUCTION

Ceramic high-temperature fuel cell and electrolyser are efficient energy-conversion systems for electrical power generation and hydrogen production. Thanks to their high flexibility in terms of technological applications, the same device can be alternatively used in fuel cell and steam electrolysis modes (i.e. in Solid Oxide Fuel Cell or Electrolysis Cell, SOFC or SOEC). This type of high-temperature electrolyser-fuel-cell device is constituted by a stack of elementary Solid Oxide Cells (SOCs), each one being composed of a dense electrolyte sandwiched between two porous electrodes. The microstructure of the electrodes plays a major role in the global cell performances by controlling the rates of the electrochemical reactions. Nevertheless, electrodes present a complex three dimensional microstructure that is submitted to numerous functional constrains, such as maximizing electrochemical reactive sites while increasing gas, electronic and ionic transport properties. From that point of view, the electrode microstructural optimization is crucial to improve all together the performances and the durability of SOCs. However, the basic relationships between the three-dimensional characteristics of the microstructure and the electrode properties are not still precisely understood. In the objective to better understand such relations, a method able to generate representative virtual microstructures will be especially helpful. In this article, a method based on the 'Gaussian Random Field' approach is detailed and validated on real 3D electrode reconstructions.

[*] Corresponding author at: Univ. Grenoble Alpes – CEA/LITEN, 17 Rue des Martyrs 38054 Grenoble, France.
E-mail: hamza.moussaoui@cea.fr (H. Moussaoui)

2. IMAGE ACQUISITIONS & CHARACTERIZATION

2.1 Materials and sample preparation for X-ray tomography

Sample investigated in the present work was taken from commercial cell. The oxygen electrode is constituted by a porous Mixed Ionic-Electronic Conductor (MIEC) of Lanthanum Strontium Cobalt Ferrite (LSCF). The hydrogen electrode is a cermet composed of a pure ionic conductor of Yttria-Stabilized Zirconia (YSZ) and an electronic conductor of Ni. It is worth mentioning that this study examines the active layer of this latter electrode in its reduced state.

Adequate sample preparation for X-ray nano-tomography is of central importance for accurate measurements. Both size and geometry of the sample impact the quality of the projections recorded during a scan. A thin sample is required to limit absorption. In contrast, a sufficiently large volume is necessary to be representative for the main morphological properties of the complete electrode. In this study, the samples have been prepared with a Plasma-FIB Vion (FEI^{TM}) using an inductively coupled plasma source of Xe^+ ions [1].

2.2 X-ray nano-tomography procedure

Image acquisition has been carried out at the new ID16A Nano-Imaging beamline of the European Synchrotron Radiation Facility (ESRF). The tomography procedure is based on an optical phase contrast imaging technique that follows a holotomographic scheme [2]. This method is well adapted to separate the porosity as well as the different solid phases [3-4]. It can be noticed that these volumes are sufficiently large to be statistically representative for the studied heterogeneous media. Indeed, the Representative Volume Elements (RVEs) are roughly equal to 15 x 15 x 15 μm^3 and 9 x 9 x 9 μm^3 for the Ni-YSZ cermet and the LSCF electrode respectively [5]. The beam's energy used in these experiments is as high as 33.6keV. The spatial resolution has been estimated at ≈ 50 nm by analysis of the gray level profile across the interface between the solid and pore phases [1]. It is worth mentioning that this resolution is fine enough to describe the fine microstructure of the electrodes.

2.3 Microstructure characterization

Once the 3D reconstructions were obtained, a set of numerical tools has been used to characterize as objectively as possible the morphology and the physical behavior of the microstructures. Thus, in-house Matlab® programs have been implemented in this frame. It is worth highlighting that all the studied volume sizes are high enough to be statistically representative for the whole electrodes. Moreover, the isotropy in the morphological properties has been fulfilled. Consequently, all the properties presented hereafter are an averaging of the values along the three spatial directions.

2.3.1 Morphological measurements

Morphological measurements include mainly the covariance function, the phase size distribution, the geometric tortuosity, constrictivity and the density of Triple Phase Boundary lengths (TPBls).

The covariance function shows how the phase is distributed in the 3D space. It is considered as the footprint of the microstructure as it contains the most relevant information of the microstructure. In a mathematical point of view, it is the probability that two points distant by a distance h belong to the same phase X:

$$C_X(h) = P(x \in X, x + h \in X) \tag{1}$$

We recall here some properties of this function:

$$\begin{aligned} &0 \le C_X(h) \le f_X = C_X(0) \\ &\lim_{h \to +\infty} C_X(h) = f_X^2 \end{aligned} \tag{2}$$

where f_X is the volume fraction of the phase X.

Phase Size Distribution (PSD), also called granulometry, is computed using morphological openings with homothetic spheres as structuring elements as detailed by J. Serra [6].

The specific surface area S_p of a phase X is defined simply as the total surface area of the interface between this phase X and its complementary X^c, normalized by the volume fraction of this phase [5]. The mean phase diameter d_p is also computed for each phase using its granulometry.

The geometric tortuosity τ^{geo} takes into account the fact that transport in one phase (heat and mass) is hampered since the pathway for diffusion is not straight but sinuous and entangled. It is defined simply by the ratio of the length of the curve to the distance between the ends of it.

The geometric constrictivity β is a dimensionless parameter with values between 0 (e.g. for trapped pores) and 1 (e.g. for cylindrical pores with constant radius) [7]. It contributes to a transport resistance caused by some flux constriction effects since the cross section area for diffusion is not constant. This parameter describing the 'bottleneck' phenomenon can be simply defined as the ratio of minimum over maximum cross section area.

Since the gas and charge species can only flow within the connected network, only the connected phases contribute to the overall cell efficiency, the volume percentage of the connected phase ε is then calculated for each phase.

Finally, the TPB lengths correspond to the lines in the Ni-YSZ microstructure where the ionic, electronic and gas phases meet. They are of central importance since they correspond to the sites for the electrochemical reactions [5].

2.3.2 Physical characterization

Gas diffusion through the open porosity and charge transport through the connected ionic and electronic conducting phases are strongly hindered by the complex microstructure of the electrodes. Thus, 'intrinsic' gas diffusivities or charge conductivities are much higher than their effective values in the electrode microstructure. Therefore, an 'apparent tortuosity factor' τ^{app} is defined in chemical science engineering as [8]:

$$\tau_X^{app} = (\varepsilon_X f_X) \frac{D_X^{bulk}}{D_X^{eff}} \tag{3}$$

where D_X^{bulk} and D_X^{eff} are the charge conductivity (for the solid phase) or gas diffusivity (for the porous phase) of the bulk (dense material) and the porous material respectively.

One way to determine the effective coefficients is by employing some homogenization techniques as detailed by J. Laurencin et al. [8]. These methods aim to replace a three-dimensional representation of the real heterogeneous electrode by an equivalent homogeneous medium characterized by its effective properties. In this study, Finite Element Method (FEM) simulations have been employed to solve the Laplace's equations for gas diffusion or charge transfer.

It is worth noting that the 'apparent' tortuosity corresponds to a purely phenomenological representation of the microstructure morphology, and encompasses both the geometric tortuosity τ^{geo} and the constrictivity factor β [7-8].

3. TWO-PHASE MATERIALS MODEL

We will try now to build a synthetic microstructure that is morphologically and physically equivalent to the real microstructure reconstructed in the European Synchrotron Radiation Facility, and described in part 2.

Many geometrical models can be used to build synthetic microstructures; 'Random Set Models' for example involves generating the phases by spatially combining geometrical random sets (e.g. union of uniformly dispersed spheres of random radius) [9-14]; 'Random Field Models' however consists in generating a spatial random field assigning a random gray level to each voxel. This field is afterwards truncated by thresholding [15-18].

We chose to use the Gaussian 'Random field model' over its simplicity and nearly immediate code execution. A convenient way to produce these simulations is to work in Fourier space as it makes operations easier [19].

The microstructure is generated by the convolution of a Gaussian random field U with a weight function ω as described for the first time by Alder et al. [17] and further developed by Liang et al. [18]. The resulting field Z_X is thresholded. The value of the threshold λ_X is chosen to reproduce the measured volume fraction f_X of the phase.

For the set X, we use:

$$X = \{x; Z_X(x) \geq \lambda_X\} \tag{4}$$

$$Z_X(x) = (w_X * U)(x), \quad U \sim \mathcal{N}(0,1) \tag{5}$$

where $*$ is the convolution operator, λ_X is the threshold and U(x) follows the normal distribution $\mathcal{N}(0, 1)$ of mean 0 and variance 1. The expectation of the indicator function of the random set X leads to:

$$f_X = P\{Z_X(x) \geq \lambda_X\} = P\{N(0,1) \geq \lambda_X\} \tag{6}$$

This equation provides the threshold λ_X. Indeed:

$$\lambda_X = F^{-1}(1 - f_X) \tag{7}$$

where F is the cumulative distribution function of the normal distribution and the volume fraction f_X is given by measurements on the real image.

The weight function, normalized and symmetric, is related to the covariance function $C_X(h)$ of X by [15] [20]:

$$C_X(h) = \frac{1}{2\pi} \int_0^{\sigma_X(h)} \frac{1}{\sqrt{1-t^2}} e^{-\frac{\lambda_X^2}{1+t}} dt \tag{8}$$

where $\sigma_X(h) = (w_X * w_X)(h)$. The function w_X is thus obtained by using:

$$\omega_X = FFT^{-1}(\sqrt{FFT(\sigma_X)}) \tag{9}$$

with FFT referring to the discrete Fast Fourier Transform, and FFT^{-1} its inverse form.

The only data we need to extract from the real microstructure is its covariance function C_X of the solid phase. Then 4 steps are necessary to generate the final microstructure:

1. Generate a non-correlated Gaussian random field with null expectation and unit variance $U(x) \sim \mathcal{N}(0,1)$
2. Compute the threshold λ_X (c.f. eq 7)
3. Introduce a correlation to the random field to produce Z_X (c.f. eq 5). Note that σ_X is obtained by inverting numerically the equation relating σ_X to C_X and λ_X.

It is worth mentioning that our numerical model includes a step of fitting a discrete correlation function σ_X. It has been found that the mean of three Gaussian functions with different correlation lengths gave the best fitting. The use of only one Gaussian function seems to be less relevant in our case and leads to a significant error on the fit especially for the Ni-YSZ electrode. Moreover, a linear interpolation of the discrete correlation function induces a noise at the interface between phases. In fact the fitting function should fulfill some conditions as detailed by C. Lantuéjoul [20].

4. Thresholding: the resulting field Z_X is finally thresholded with the value λ_X to get X.

4. MODEL EXTENSION TO THREE-PHASE MATERIALS

Three-phase synthetic microstructures are modeled using two underlying independent truncated random fields X and Y [4]. Each truncated random field X and Y is created as described in the previous section on two-phase materials. In order to obtain the final synthetic three-phase (A_1, A_2, A_3) microstructure we consider the following combination of the two random sets X and Y:

$$A_1 = X\,, \qquad A_2 = X^c \cap Y\,, \qquad A_3 = X^c \cap Y^c \tag{10}$$

Each field A_i (i=1,2,3) is used to represent either the porous, Ni or YSZ phase. Then we have six possible combinations for the attribution of these three phases. In practice, the best combination will be retained.

The covariance functions of the two underlying random sets read:

$$C_X(h) = C_{A_1}(h) \;\; ; \;\; C_Y(h) = \frac{C_{A_2}(h)}{C_{A_1}(h)} \tag{11}$$

where: $$\overline{C}_{A_1}(h) = C_{A_1^c}(h) = 1 - 2C_{A_1}(0) + C_{A_1}(h) \quad (12)$$

Consequently, we can apply the same procedure (as previously detailed) to generate the two random fields Z_X and Z_Y. Thereafter, the thresholds λ_X and $\lambda_Y$will give the random sets X and Y. Using equation (10), we retrieve the three phases (pore, Ni and YSZ).

5. RESULTS AND DISCUSSIONS

In order to validate the representativeness of our synthetic microstructures, a set of key parameters is carefully analyzed. For each couple of real and synthetic media, the covariance function, phase size distribution, and finally all subsequent morphological and physical parameters are computed and the gap is discussed.

Taking into account the stochastic aspect of our model, first we generated several synthetic microstructures and we chose the one that fitted best the real covariance function. The error was always small whatever the realization as we used a volume large enough to be statistically representative.

5.1 Two-phase materials

A first visual inspection seems to indicate that the synthetic microstructure is quite similar to the real one (Fig. 1). This statement is confirmed by the comparison of the covariance functions computed for the synthetic and real microstructures. As shown in Fig. 2a, a very good agreement is found for both phases meaning that the method allows generating a representative microstructure. To go further in the validation, the phase size distributions or granulometry plots are given in Fig. 2b. As expected, the curves of the virtual and the real microstructures present a similar shape. Nevertheless, it can be noticed that the porosity distribution of the real microstructure is slightly wider than the synthetic one. This slight discrepancy in the phase size distribution is liable to affect some of the morphological parameters of the synthetic microstructure. All these parameters are listed in table I and compared to the ones measured on the 3D electrode reconstruction. Firstly, it worth noting that the overall error on the computed properties are rather negligible. Thus, it allows validating the method to generate valuable synthetic microstructure for the SOC oxygen electrode. Nevertheless, the highest mismatch is found on the geometrical tortuosity and the constrictivity parameter leading to an error of around 10% on the 'apparent' tortuosity factor of the solid phase. This discrepancy on tortuosity and phase constriction is well correlated with the difference in granulometry between the synthetic and real microstructure. It means that the model would be not able to catch a microstructure with a highly tortuous phase or with high constriction effects.

Despite this slight mismatch in tortuosity and constrictivity, it can be claimed that the Gaussian 'Random Field' model mimics accurately this typical real microstructures of SOCs oxygen electrode. In general point of view, the method is able to represent the continuous network of each phase as shown in Fig. 1. Other methods based on sphere packing usually fail to reproduce this feature of the sintered porous electrode since they tend to keep in the final microstructure the geometry of the initial spheres [10] [14].

The validation of this tool on other cell electrodes with different microstructures is ongoing, and it will be used afterwards to investigate the morphological relationships between the microstructure parameters.

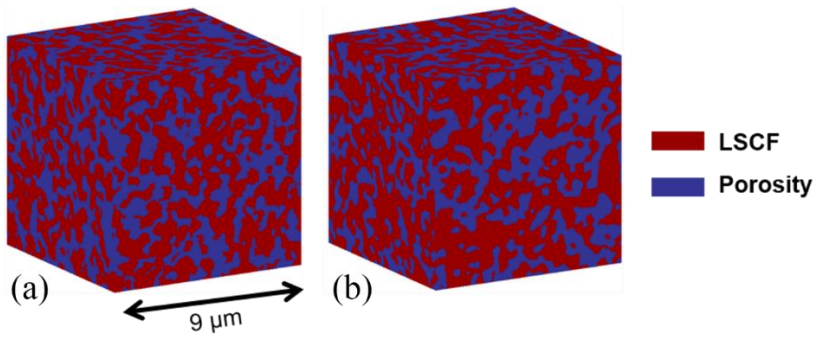

Figure 1. Visual comparison of the real microstructure (a) and the synthetic microstructure (b) of the oxygen electrode's microstructure.

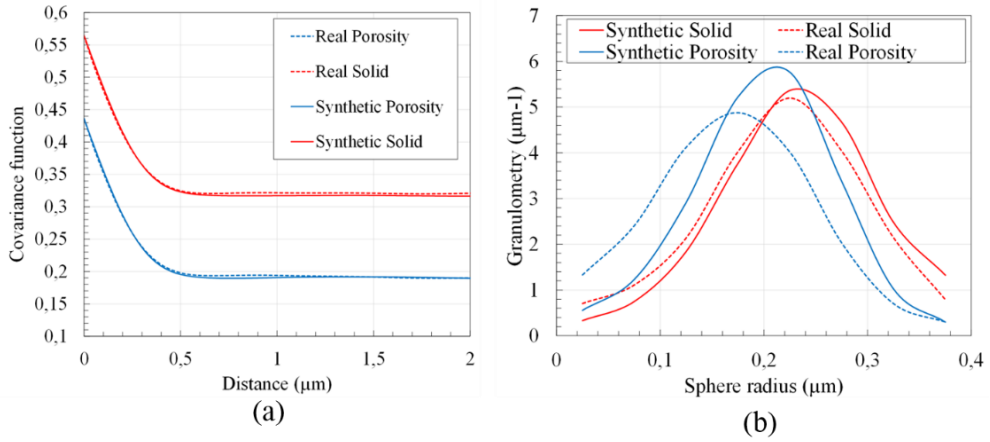

Figure 2. Quantitative comparison of the covariance function (a) and granulometry (b) of the two phases between the synthetic and the real microstructures.

Table 1. Summary of the validation of the morphological and physical parameters.

	Porous phase						**LSCF phase**						
Parameter	f (%)	ε (%)	d_p (µm)	τ^{geo} (-)	β (-)	τ^{app} (-)	f (%)	ε (%)	d_p (µm)	τ^{geo} (%)	β (-)	τ^{app} (-)	S_p (μm^{-1})
Real µ-structure	43.63	99.97	0.37	1.22	0.14	2.25	56.37	99.99	0.44	1.36	0.23	1.95	3.62
Synthetic µ-structure	43.57	99.93	0.40	1.24	0.15	2.37	56.43	99.98	0.46	1.47	0.24	1.77	3.45
Error (%)	0%	0%	7%	2%	7%	5%	0%	0%	5%	8%	4%	10%	5%

5.2 Three-phase materials

For the three-phase model, six combinations are possible as shown in the previous section. All the six combinations have been generated and compared. No significant difference has been found whatever the choice of the combination. However, the numerical phase generated from the first random field A_1 presents the best results whereas the other complementary phases deduced by set operations (cf. eq. (10)) are less representative for the real microstructure. To illustrate this phenomenon, the Ni-YSZ synthetic microstructure provided in Fig. 3 have been generated considering the pore phase ascribed to the 'first' random set A_1 (Pore=A_1, YSZ=A_2, Ni=A_3). As shown on Fig. 4a, the covariance function for the porosity matches perfectly the one of the reconstructed electrode. However, a noticeable difference arises for the 'third' created phase corresponding to Ni. The slight mismatch on the Ni covariance function is consistent with the simple visual inspection of the 3D synthetic and real volumes. Indeed, the 3D rendering volumes given in Fig. 3 reveal that the two microstructures present some morphological differences. This is confirmed by the PSD curves plotted in Fig. 4b: the granulometries of the pore and Ni phases for the real microstructure are much widespread than those measured on the synthetic volume. In other words, the three PSDs of the virtual microstructure present less variability compared to the reality.

As already discussed for the oxygen electrode, the mismatch in PSD is accompanied by some substantial differences for the microstructural parameters listed in Table 2 The main error is found on the constrictivity factor, and hence on the 'apparent' tortuosity factor, for both the Ni and porous phases. Indeed, as suspected for the oxygen electrode, the method presents some limitations to generate microstructure that mimics phases with low constrictivity factor (i.e. high constriction effect). Note that the low values reported for the Ni and YSZ phases for the real microstructure are simply correlated to their low volume fractions of around 28% (compared to 44% for YSZ). In spite of this limitation, the density of TPBs has been successfully retrieved with the model. Indeed, an error of around 11% has been found for this parameter. Therefore, it can be concluded that the method remains valid even for the hydrogen electrode composed of three phases. As for the oxygen electrode, other methods based on sphere packing have been already used to generate this Ni-YSZ electrode [11-14]. However, from our best knowledge, no direct comparison with real microstructure has been done. As discussed for

the oxygen electrode, it can be suspected that the current description of the phase by set of overlapping spheres requires some improvement to be fully adapted regarding the morphology of the SOCs electrodes.

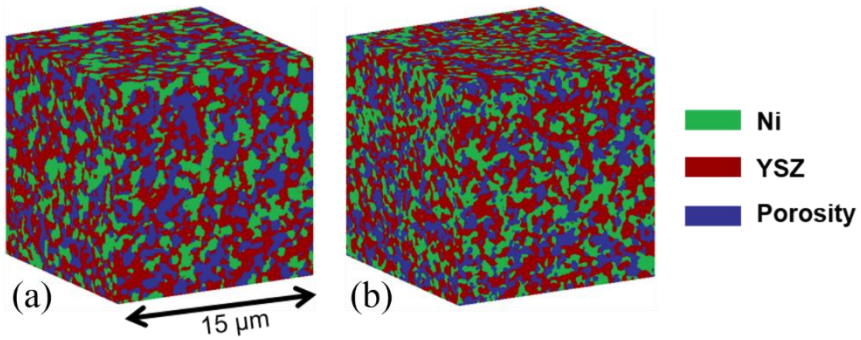

Figure 3. Visual comparison of the real microstructure (a) and the synthetic microstructure (b) of the oxygen electrode's microstructure.

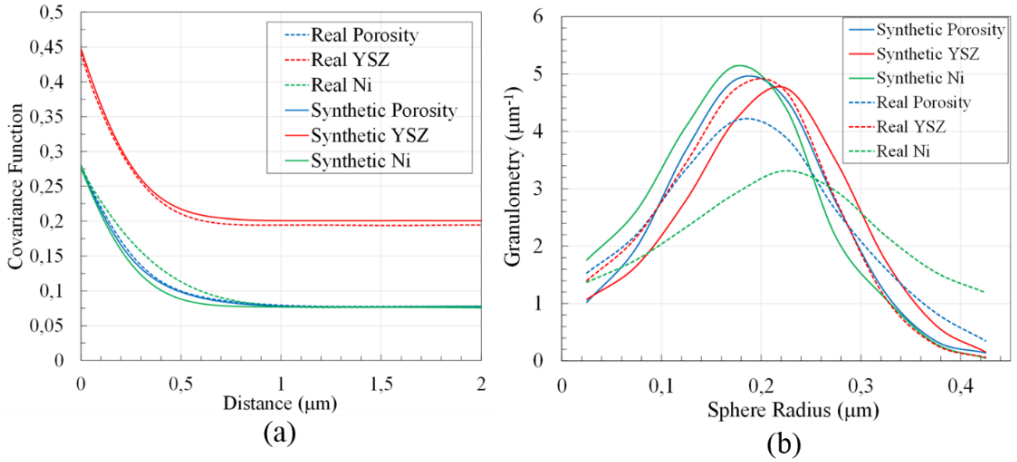

Figure 4. Quantitative comparison of the covariance function (a) and granulometry (b) of the three phases between the synthetic and the real microstructures.

Table 2. Summary of the validation of the morphological and physical parameters.

	Porous phase							**YSZ phase**						
Parameter	f (%)	ε (%)	d_p (µm)	S_p ($µm^{-1}$)	τ^{geo} (-)	β (-)	τ^{app} (-)	f (%)	ε (%)	d_p (µm)	S_p ($µm^{-1}$)	τ^{geo} (-)	β (-)	τ^{app} (-)
Real µ-structure	28.04	94.74	0.39	2.67	1.67	0.09	9.67	44.08	99.78	0.36	3.68	1.43	0.13	2.29
Synthetic µ-structure	27.58	98.64	0.38	2.55	1.61	0.12	5.22	44.75	99.92	0.40	3.47	1.44	0.13	2.28
Error (%)	2%	4%	3%	4%	4%	33%	46%	1%	0%	11%	6%	1%	0%	0%

	Ni phase							
Parameter	f (%)	ε (%)	d_p (µm)	S_p ($µm^{-1}$)	τ^{geo} (-)	β (-)	τ^{app} (-)	TPBL density ($µm^{-2}$)
Real µ-structure	27.88	97.45	0.47	2.30	1.75	0.08	6.95	4.78
Synthetic µ-structure	27.67	99.32	0.34	2.85	1.80	0.13	4.60	5.31
Error (%)	1%	2%	38%	24%	3%	38%	34%	11%

6. CONCLUSION AND PROSPECTS

A methodology has been implemented for simulating 3D SOC electrodes microstructure by means of Gaussian 'Random Field' model. The representativeness of the resulting synthetic microstructures has been validated by comparing them to the real microstructures reconstructed by X-ray nano-tomography. The experiments have been performed at the new Nano-Imaging beamline ID16A-NI at the European Synchrotron Radiation Facility (ESRF) enabling us to obtain large field of view while maintaining a high spatial resolution. It has been shown that the method is able to mimic accurately the two-phase oxygen electrode microstructure composed of porous LSCF. The model has been also extended to the three-phase hydrogen electrode composed of porous Ni-YSZ. It has been found that the method remains valid for this electrode. However, the analysis has revealed that the method fails to perfectly reproduce highly tortuous and constricted phase geometries.

Work is ongoing to overcome this restriction, either by adapting this model or by using a different 'Random Set' Model including stochastic overlapping sphere distributions. However, it should be kept in mind that no model is able to generate synthetic volumes representative of the large variety of SOC electrodes microstructures. From that point of view, coupling two models could be a promising way to encompass a wider range of material microstructures.

REFERENCES

[1] M. Hubert, J. Laurencin, P. Cloetens, J.C. da Silva, F. Lefebvre-Joud, P. Bleuet, A. Nakajo, E. Siebert, "Role of microstructure on electrode operating mechanisms for mixed ionic electronic conductors: From synchrotron-based 3D reconstruction to electrochemical modeling," Solid State Ionics 294, 90-107 (2016).

[2] P. Bleuet, G. Audoit, J.-P Barnes, J. Berteau, et al., "Specifications for Hard Condensed Matter Specimens for Three-Dimensional High-Resolution Tomographies," Microscopy and Microanalysis, 19(3), 726-739 (2013).

[3] J. Laurencin, et al., "Characterisation of Solid Oxide Fuel Cell Ni–8YSZ substrate by synchrotron X-ray nano-tomography: from 3D reconstruction to microstructure quantification," J. Power Sources, 198, 182-189 (2012).

[4] P. Cloetens, W. Ludwig, J. Baruchel, et al., "Holotomography: Quantitative phase tomography with micrometer resolution using hard synchrotron radiation x rays," Applied Physics Letters, 75(19), 2912-2914 (1999).

[5] F. Usseglio-Viretta, J. Laurencin, G. Delette, J. Villanova, et al., "Quantitative microstructure characterization of a Ni–YSZ bi-layer coupled with simulated electrode polarization," J. Power Sources, 256, 394-403 (2014).

[6] Jean Serra, [Image Analysis and Mathematical Morphology], Academic Press, (1988).

[7] L. Holzer, D. Wiedenmann, B. Münch, L. Keller, M. Prestat, et al., "The influence of constrictivity on the effective transport properties of porous layers in electrolysis and fuel cells," J. Mater. Sci., 48(7), 2934–2952 (2013).

[8] J. Laurencin, J. Mougin, [Hydron Production by Electrolysis], Wiley, Munich & Gliwice, 191-272 (2015).

[9] K. Rhazaoui, Q. Cai, P. Shearing, C.S. Adjiman, N.P. Brandon, "Solid Oxide Fuel Cell Electrode 3D Microstructure and Performance Modeling," ECS Transactions, 35(1), 1097-1105 (2011).

[10] X. Liu, C.L. Martin, G. Delette, J. Laurencin, D. Bouvard, T. Delahaye, "Microstructure of porous composite electrodes generated by the discrete element method," J. Power Sources, 196(4), 2046–2054 (2011).

[11] X. Liu, C.L. Martin, G. Delette, J. Laurencin, D. Bouvard, T. Delahaye, "Microstructure of porous composite electrodes generated by the discrete element method," J. Power Sources, 196(4), 2046–2054 (2011).

[12] A. Bertei, B. Nucci, C. Nicolella, "Microstructural modeling for prediction of transport properties and electrochemical performance in SOFC composite electrodes," Chemical Engineering Sci., 101, 175–190 (2013).

[13] Qiong Cai, Claire S. Adjiman, Nigel P. Brandon, "Modelling the 3D microstructure and performance of solid oxide fuel cell electrodes: Computational parameters," Electrochimica Acta, 56(16), 5804–5814 (2011).

[14] H. Choi, D. Gawel, A. Berson, et al., "Comparison between FIB-SEM Experimental 3-D Reconstructions of SOFC Electrodes and Random Particle-Based Numerical Models," ECS Transactions, 35(1), 997-1005 (2011).

[15] B. Abdallah, F. Willot, D. Jeulin, "Morphological modelling of three-phase microstructures of anode layers using SEM images," Journal of Microscopy, 263(1), 51-63 (2016).

[16] F. Bron, D. Jeulin, "Modelling a food microstructure by random sets," Image Anal Stereol, 23, 33-44 (2004).

[17] P.M. Alder et al., "Flow in simulated porous media" Int. J. Multiphase Flow, 16(4), 691-712(1990).

[18] Z.R. Liang, C.P. Fernandes, F.S Magnani, P.C. Philippi, "A reconstruction technique for three-dimensional porous media using image analysis and Fourier transforms," J. of Petrol. Sci. Eng., 21(3-4), 273-283 (1998).

[19] A. Lang, J. Potthoff, "Monte Carlo Methods and Applications," 17(3), 195-214 (2011).

[20] Christian Lantuéjoul, [Geostatical Simulation: Models and Algorithms], Springer, New York, 183-220 (2002).